

# Gross photosynthesis and lake community metabolism during the spring phytoplankton bloom

David J. Suggett<sup>1</sup>

Department of Biological Sciences, University of Essex, Colchester, CO4 3SQ, United Kingdom

Stephen C. Maberly

Lake Ecosystem Group, CEH, Lancaster Environment Centre, Library Avenue, Bailrigg, Lancaster, LA1 4AP, United Kingdom

Richard J. Geider

Department of Biological Sciences, University of Essex, Colchester, CO4 3SQ, United Kingdom

## Abstract

Daily productivity determinations of linear photosynthetic electron transfer and of net and gross inorganic CO<sub>2</sub> uptake were determined in situ throughout a 6-week sampling period of the spring phytoplankton bloom in Esthwaite Water in the English Lake District. Photosynthetic electron transfer rates, expressed as gross O<sub>2</sub> evolution, were determined from fast repetition rate (FRR) fluorometry and discrete laboratory measurements of the photosynthetic unit size. These gross O<sub>2</sub> evolution determinations were also made free from contemporaneous dark-adapted FRR measurements and the need for sample blanks. Net and gross CO<sub>2</sub> uptake was determined from changes in total inorganic carbon calculated from in situ pH measurements. Two phases to the bloom were observed. An initial bloom was dominated by the diatom *Asterionella formosa*, while a secondary phase was characterized by an increase in flagellates and cyanobacteria. For both phases, daily FRR-based gross O<sub>2</sub> evolution and pH-based gross CO<sub>2</sub> uptake were tightly coupled, suggesting that daily gross O<sub>2</sub> production was driving daily changes in CO<sub>2</sub> assimilation and thus in community metabolism. This is the first investigation to show closely related rates of gross O<sub>2</sub> production and CO<sub>2</sub> uptake measured in situ.

Daily phytoplankton production is determined routinely in aquatic studies to examine ecosystem energetics. Typically, daily production is estimated from discrete incubations of natural material. However, this approach may give rise to considerable error because realistic environmental conditions may not be reproduced in the incubation bottles (Wilhelm et al. 2004). Various techniques are now used to provide direct, in situ measures of primary productivity. These include diel O<sub>2</sub> (Gelda and Effler 2002) and CO<sub>2</sub> (Maberly 1996) exchange, and fast repetition rate (FRR) fluorescence (Kolber et al. 1998; Suggett et al. 2001; Raateoja et al. 2004). Direct in situ O<sub>2</sub> and CO<sub>2</sub> measurements yield a measure of the net daily planktonic community metabolism during the day and of net community respiration at night (del Giorgio et al. 1999; Cole et al. 2000), whereas FRR fluorescence yields the instantaneous gross phytoplankton photochemical activity (Falkowski and Kolber 1995; Gorbunov et al. 2001). We combined these techniques to examine the transfer of energy from photons to carbon dioxide fixation in situ.

<sup>1</sup> Corresponding author (dsuggett@essex.ac.uk).

## Acknowledgments

We thank Mark Moore for providing assistance with high-performance liquid chromatography pigment measurements and Mitzi de Ville and Julie Parker for assistance with field sampling. Insightful comments from Marcel Babin, Mark Moore, and two anonymous referees considerably improved this paper. The National Environmental Research Council U.K. supported this work (NER/A/S/2000/01237).

Continuous in situ measurements of FRR fluorescence and pH were used to estimate daily phytoplankton productivity at a single depth throughout a 6-week sampling period of the 2003 spring bloom in Esthwaite Water in the English Lake District. We describe continuous FRR-based productivity determinations that are free from additional dark-adapted fluorescence and sample blank measurements and incorporate photosynthetic unit size measurements from natural samples. Here we show that the gross photosynthesis measured by FRR and gross daily community productivity estimated from diel changes of TCO<sub>2</sub> covaried in two phases of the spring bloom. The first phase was almost exclusively dominated by the diatom *Asterionella formosa*, whereas the second phase was characterized by increased numbers of flagellates, in particular *Rhodomonas* spp. and *Chrysochromulina parva*, and the cyanobacterium *Anabaena circinalis*. Our results demonstrate tight coupling of gross photosynthetic electron transfer rates with gross community metabolism. Different photosynthetic quotients were observed for the two phases of the spring bloom corresponding with the change in phytoplankton community structure.

## Methods

Sampling was conducted from 28 February to 14 April 2003 in Esthwaite Water in the English Lake District (54°22'N 2°59'W). During these 6.5 weeks, we experienced two distinct phases of the spring bloom, an initial bloom in weeks 1–2.5 (phase 1) and a secondary bloom of lower

Table 1. Symbols, terms and definitions (derivations). Fluorescence parameters follow Kromkamp and Forster (2003) and Suggett et al. (2003). All fluorescence parameters are in instrument units unless stated otherwise. PSII and RCII are photosystem II and reaction centers of PSII, respectively.

Symbol	Term	Definition or derivation
$F_o$	Minimum fluorescence under dark adaptation	
$F_o'$	Minimum fluorescence under ambient light	
$F_o'^{FRR}$	Minimum fluorescence under ambient light in the FRR enclosed chamber	
$F'$	Steady-state fluorescence in the FRR open chamber	
$F_m$	Maximum fluorescence under dark adaptation	
$F_m'$	Maximum fluorescence under ambient light	
$f^m$	“Background” fluorescence	
$F_v/F_m$	Maximum PSII photochemical efficiency under dark adaptation (dimensionless)	$= (F_m - F_o)/F_m$
$F_v'/F_m'$	Maximum PSII photochemical efficiency under ambient light (dimensionless)	$= (F_m' - F_o')/F_m'$
$F_q'/F_m'$	PSII photochemical efficiency under ambient light (dimensionless)	$= (F_m' - F')/F_m'$
$Q_A^{OX} : Q_A^{TOTAL}$	PSII efficiency factor or the ratio of effective to maximum trapping efficiency (dimensionless)	Proportion of $Q_A$ molecules that are oxidized $= (F_m' - F')/(F_m - F_o^{FRR})$
$\sigma_{PSII}$	PSII effective absorption cross section under dark adaptation ( $\text{\AA}^2 \text{ photon}^{-1}$ )	Rate of $Q_A$ oxidation and thus of closure of PSII reaction centers
$\sigma_{PSII}'$	PSII effective absorption cross section under ambient light in either FRR chamber ( $\text{\AA}^2 \text{ photon}^{-1}$ )	
$\sigma_{PSII}^{abs}'$	Spectrally adjusted PSII effective absorption cross section under ambient light in either FRR chamber ( $\text{\AA}^2 \text{ photon}^{-1}$ )	Eq. 3
$n_{O_2}$	Reciprocal of the Emerson and Arnold number ( $\text{mol O}_2 [\text{mol Chl } a]^{-1}$ )	Single-turnover flash-induced $O_2$ evolution per unit Chl $a$
$E_o, E_{od} (PAR)$	Incident irradiance, incident downwelling photosynthetically active radiation ( $\mu\text{mol photons m}^{-2} \text{ s}^{-1}$ )	
$P_{O_2}^{chl}$	FRR-based $O_2$ evolution rate per unit Chl $a$ ( $\text{mol O}_2 [\text{g Chl } a]^{-1} \text{ h}^{-1}$ ),	Eq. 4
$\sum P_{O_2}^{GROSS}$	Daily integrated FRR-based $O_2$ evolution rate per unit volume ( $\text{mol O}_2 \text{ m}^{-3}$ )	Eq. 5
$TCO_2$	Total concentration of inorganic carbon as free $CO_2$ , $HCO_3^-$ , and $CO_3^{2-}$ ( $\text{mol CO}_2 \text{ m}^{-3}$ )	Eq. 6
$\sum P_{CO_2}^{NET}, \sum P_{CO_2}^{GROSS}$	pH-based daily net, gross $CO_2$ uptake per unit volume ( $\text{mol CO}_2 \text{ m}^{-3}$ )	Eq. 7, 9

magnitude in weeks 4–6.5 (phase 2). These two phases will be referred to throughout.

**FRR fluorescence and photosynthetic unit size**—A Chelsea Instruments FAST<sup>tracka</sup> FRR fluorometer (SN 182039) was attached to a mooring at a depth of 1 m. A  $2\pi$  collector measuring downwelling photosynthetically active radiation,  $E_{od} (PAR)$  (400–700 nm), was integrated with the FRR fluorometer and positioned at the same depth as the excitation-emission optical windows. A second PAR sensor was mounted on the mooring,  $\sim 2$  m above the water surface, to continually log incident PAR. Chlorophyll  $a$  (Chl  $a$ ) concentration can typically exceed 20–30  $\text{mg m}^{-3}$  in the spring, yielding fluorescence levels that saturate the photomultiplier tube of the FAST<sup>tracka</sup> even when the gain is set to the minimum sensitivity. Therefore, the FAST<sup>tracka</sup> FRR fluorometer was set to a gain of 1, and a neutral density filter was placed over the window between the sample and photomultiplier tube throughout the sampling period. Use of a neutral density filter did not significantly alter the variable fluorescence signal when tested with various algal species in the laboratory (data not shown).

FRR fluorescence was acquired continuously for both open (exposed to ambient light) and enclosed (dark) chambers at hourly intervals, except during weeks 1–2, when intermittent battery failure resulted in a sparse record. The fluorometer was serviced twice a week to clean optical windows, replace neutral density filters, download data, and change the battery. Surface-water samples were collected during each service and returned to the laboratory for immediate measurements of photosynthetic unit size, pigments, and optical absorption. The underwater spectral light field at a depth of 1 m was measured every 2 weeks with a Macam 9050 spectroradiometer. Each spectrum was recorded between 400 and 700 nm at a 1-nm interval.

Each FRR acquisition consisted of 15 single-turnover excitation sequences set according to Suggett et al. (2003, 2004). Hourly acquisitions were processed by v4 software (Sam Laney pers. comm.) to generate values of minimum and maximum fluorescence and the effective absorption cross section (Table 1). Connectivity was also retrieved from the v4 software but varied only slightly (0.28–0.32, dimensionless) throughout the investigation. Fluorescence parameters were adjusted for instrument-specific response,

scatter, and baseline functions during v4 processing essentially as described by Laney (2003).

Under dark-adapted conditions, the minimum and maximum fluorescence and maximum effective absorption, termed  $F_o$ ,  $F_m$ , and  $\sigma_{\text{PSII}}$  (Table 1), will be equal for the two FRR chambers, provided they are intercalibrated. Dark-adapted fluorescence is altered to a new steady state by activation of photochemical and nonphotochemical pathways under ambient light. Consequently, different fluorescence parameters are obtained under ambient light, the majority of which are denoted by a prime (') symbol. Maximum fluorescence and the effective absorption cross section under ambient light are termed  $F_m'$  and  $\sigma_{\text{PSII}'}$ , respectively, for both FRR chambers (Table 1). We only used the  $\sigma_{\text{PSII}'}$  from the enclosed chamber because potential scattering of contaminating ambient red light was vastly reduced, thus improving the signal-to-noise ratio to yield a more robust fitting procedure used in calculating  $\sigma_{\text{PSII}'}$ . Minimum fluorescence under ambient light is equal to the steady-state fluorescence in the FRR open chamber, termed  $F'$  (Table 1), but not in the FRR enclosed chamber. Here, we term the minimum fluorescence under ambient light in the enclosed chamber  $F_o'^{\text{FRR}}$  (Table 1). The PSII photochemical efficiency was calculated as  $(F_m - F_o)/F_m$  ( $=F_v/F_m$ ) or  $(F_m' - F')/F_m'$  ( $=F_v'/F_m'$ ) for dark-adapted and steady-state (ambient light) conditions, respectively (Table 1). Maximum and minimum fluorescence yields and hence values of PSII photochemical efficiency were then adjusted for the proportion of nonactive background fluorescence.

Sample blanks were calculated from separate laboratory FRR measurements on filtrates of discrete dark-adapted samples (Suggett et al. 2004; Moore et al. 2005) to yield the proportion of nonactive Chl *a* fluorescence ( $f$ ). These FRR measurements were made with a second FRR fluorometer (SN 182010) that had been intercalibrated against the fluorometer used in situ and corrected for instrument-specific functions as above.  $f$  remained relatively constant throughout the sampling period,  $\sim 0.04 \pm 0.003$  (mean  $\pm$  standard error) instrument units. Consequently, the percentage contribution of nonactive fluorescence to measured  $F_m$  and  $F_o$  was highest from water samples with the lowest fluorescence yields (Fig. 1). The relationship between  $f$  and measured  $F_m$  or  $F_o$  was used to provide an approximate blank correction for FRR fluorescence yields recorded in situ because continuous blank measurements could not be made. A "true"  $F_m$  and  $F_o$  would only be measured in situ under darkness when fluorescence quenching has completely relaxed to reach a dark-adapted state. Therefore, the daily blank factor was applied from knowledge of the mean  $F_m$  and  $F_o$  the night before and after each diurnal phase.

To determine photosynthetic unit size, 4 liters of surface water were filtered onto 0.2- $\mu\text{m}$  Nuclepore filters with a gentle vacuum controlled by a hand pump. Filtration typically lasted 30–45 min. The filters were washed with a small amount of filtered lake water to resuspend the algae. Suspensions yielded final concentrations of 0.7–1.6 g Chl *a*  $\text{m}^{-3}$ ,  $\sim 40$ –160 times initial concentrations. FRR fluorescence measurements were made before and after concentration. Any samples with a significantly lower

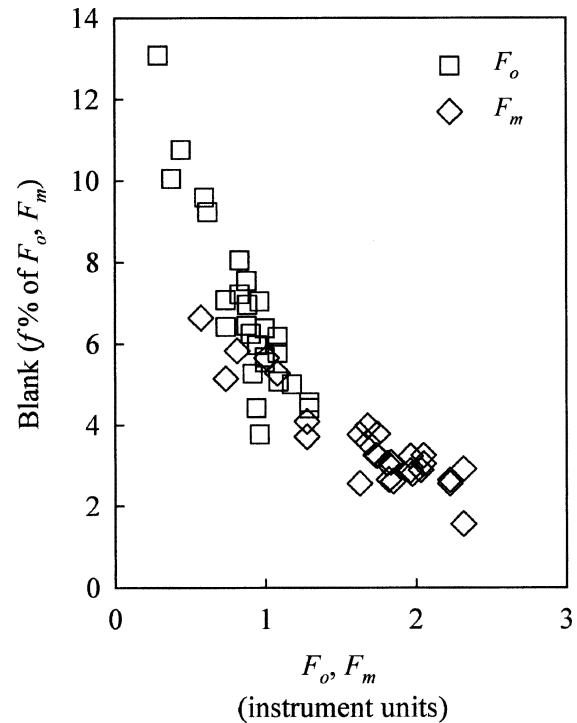


Fig. 1. Relationship between FRR fluorescence yields measured on dark-adapted samples and dark-adapted filtrate blanks. Blank fluorescence ( $f$ ) was expressed as the percentage of the absolute fluorescence yield of both  $F_o$  and  $F_m$ . A single function was fit to all data: fluorescence blank =  $-4.5924 \ln(\text{fluorescence yield}) + 5.815$  ( $r^2 = 0.875$ ,  $n = 56$ ,  $p < 0.001$ ).

blank-corrected value of  $F_v/F_m$  after concentration were assumed to have been adversely affected by the procedure and were discarded. Less than 10% of prepared samples were discarded from throughout the entire sampling period. Photosynthetic unit size was determined as described previously (Suggett et al. 2003, 2004) with a single-turnover flash approach that provides a measure of  $\text{O}_2$  evolved by the functional PSII reaction centers. Chl *a* divided by the oxygen flash yield is the Emerson and Arnold number (Falkowski and Raven 1997), termed  $\text{PSU}_{\text{O}_2}$  ( $\text{mol Chl } a \text{ (mol O}_2\text{)}^{-1}$ ). The photosynthetic unit size is a quarter of the Emerson and Arnold number under the assumption that four electron transfer events are required for each  $\text{O}_2$  evolved. We used the reciprocal of  $\text{PSU}_{\text{O}_2}$ , termed here as  $n_{\text{O}_2}$  ( $\text{mol O}_2 \text{ (mol Chl } a\text{)}^{-1}$ ), which therefore differs from the strict definition of photosynthetic unit size.

*Pigments, absorption, and microscopy*—Four aliquots of 250–500 mL from surface-water samples and two aliquots of 1–2 mL from the concentrated surface water used for measuring  $n_{\text{O}_2}$  were each filtered onto GF/F filters and divided for pigment and spectral absorption measurements. Filters were stored at  $-70^\circ\text{C}$  until analysis. Pigments were extracted into 90% acetone and analyzed according to the method of Barlow et al. (1997) on a Thermoseparations product high-performance liquid chromatographer. Chl *a* was identified by retention time and quantified from the

diode-array spectra by comparison with a pigment standard.

Absorption spectra were measured between 760 and 380 nm with a Hitachi U-3000 spectrophotometer fitted with a 60-mm integrating sphere, following the method of Ferrari and Tassan (1999). A wavelength-independent pathlength amplification coefficient obtained from mixed cultures of diatoms, dinoflagellates, chlorophytes, prasinophytes, and cyanobacteria (Cleveland and Wiedemann 1993) was applied to all samples. Absorption spectra were normalized to corresponding values of Chl *a*,  $a^{\text{Chl}}$  ( $\text{m}^2 (\text{mg Chl } a)^{-1}$ ).

Phytoplankton species composition was determined on samples preserved in Lugol iodine and counted in a Lund counting chamber with an inverted microscope (Lund 1962).

*Calculation of gross photosynthesis from FRR fluorescence*—FRR-based gross  $\text{O}_2$  production,  $p_{\text{O}_2}^{\text{chl}}$  ( $\text{mol O}_2 (\text{g Chl } a)^{-1} \text{h}^{-1}$ ), was calculated by using an approach modified from Kolber and Falkowski (1993) as the product of incident PAR ( $E_o$  (PAR),  $\mu\text{mol photons m}^{-2} \text{s}^{-1}$ , 400–700 nm), the effective absorption cross section under ambient light ( $\sigma_{\text{PSII}}'$ ,  $\text{\AA}^2 \text{ photon}^{-1}$ ), the reciprocal of the Emerson and Arnold number ( $n_{\text{O}_2}$ ,  $\text{mol O}_2 (\text{mol Chl } a)^{-1}$ ) and the proportion of primary quinone acceptor molecules,  $Q_a$ , that are oxidized (termed here  $Q_A^{\text{OX}}:Q_A^{\text{TOTAL}}$ , dimensionless) (Table 1),

$$P_{\text{O}_2}^{\text{chl}} = E_{od}(\text{PAR}) \cdot \sigma_{\text{PSII}}' \cdot Q_A^{\text{OX}}:Q_A^{\text{TOTAL}} \cdot n_{\text{O}_2} \cdot 0.0243 \quad (1)$$

It is assumed that  $E_o(\text{PAR}) \approx E_{od}(\text{PAR})$ , which is true to within less than 10% (Kirk 1994).

Here, the rate with which excitons are trapped by functional PSII reaction centers (RCIIs) is given by the product of the absorption cross section,  $\sigma_{\text{PSII}}'$ , and  $E_{od}$ . Because charge separation can only occur at open reaction centers, the rate of exciton trapping is multiplied by the proportion of total reaction centers that are open, termed  $Q_A^{\text{OX}}:Q_A^{\text{TOTAL}}$ , where  $Q_A$  is the primary electron acceptor in RCII, and  $Q_A^{\text{OX}}$  is the  $Q_A$  that are oxidized. To obtain the Chl *a*-specific photosynthesis rate, we multiply the reaction center specific rate of stable charge separation, which is given by the product of the first three terms on the right-hand side of Eq. 1, with the ratio of  $\text{O}_2$  evolved by a single-turnover saturating flash to Chl *a* ( $n_{\text{O}_2}$ ). Each saturating flash provides enough energy, and is of short enough duration, to stimulate charge separation at all RCIIs in a sample once, and only once. It is the most commonly used method for estimating photosynthetic unit size.

For Eq. 1 to balance,  $\sigma_{\text{PSII}}$  must be expressed with units of  $\text{\AA}^2 (\text{photon})^{-1}$ . The use of these units, rather than of  $\text{\AA}^2 (\text{RCII})^{-1}$ , is appropriate because the FRR fluorescence technique (Kolber et al. 1998) yields a  $\sigma_{\text{PSII}}$  that characterizes the initial slope of a plot of the fluorescence ratio  $(F - F_o)/(F_m - F_o)$  versus the cumulative photon dose. The fluorescence ratio is dimensionless, and the units

for photon dose are ( $\text{photons } \text{\AA}^{-2}$ ). Thus, the FRR fluorescence method provides measurements of  $\sigma_{\text{PSII}}$  that have units of  $\text{\AA}^2 (\text{photon})^{-1}$ .

The units for  $E_{od}$  (PAR) and  $n_{\text{O}_2}$  are  $\mu\text{mol photons m}^{-2} \text{s}^{-1}$  and  $\text{mol O}_2 (\text{mol Chl } a)^{-1}$ , respectively, while  $Q_A^{\text{OX}}:Q_A^{\text{TOTAL}}$  is dimensionless. The constant 0.0243 accounts for the conversion of  $E_{od}$  (PAR) from  $\mu\text{mol photons m}^{-2} \text{s}^{-1}$  to  $\text{mol photons m}^{-2} \text{h}^{-1}$ ,  $\sigma_{\text{PSII}}'$  from  $\text{\AA}^2 (\text{photon})^{-1}$  to  $\text{m}^2 (\text{mol photons})^{-1}$  and  $n_{\text{O}_2}$  from  $\text{mol O}_2 (\text{mol Chl } a)^{-1}$  to  $\text{mol O}_2 (\text{g Chl } a)^{-1}$ .

Our measurements of the effective absorption cross section are made at steady state (i.e., phytoplankton acclimated to ambient light conditions). Therefore,  $\sigma_{\text{PSII}}'$  in Eq. 1 accounts for nonphotochemical excitation quenching that leads to alterations of the PSII photochemical efficiency (Suggett et al. 2003).  $Q_A^{\text{OX}}:Q_A^{\text{TOTAL}}$  describes the ratio of effective to maximum trapping efficiency of photons by PSII reactions centers and accounts for photochemical alterations to the PSII photochemical efficiency. We estimated  $Q_A^{\text{OX}}:Q_A^{\text{TOTAL}}$  from measurements made in the open and enclosed FRR fluorometer chambers (Table 1, Fig 2B) as

$$Q_A^{\text{OX}}:Q_A^{\text{TOTAL}} = \frac{(F_m' - F')/(F_m' - f)^{\text{OPEN chamber}}}{(F_m' - F_o'^{\text{FRR}})/(F_m' - f)^{\text{ENCLOSED chamber}}} \quad (2)$$

The extent of photochemical quenching,  $Q_A^{\text{OX}}:Q_A^{\text{TOTAL}}$  is assumed to be given by the ratio  $(F_m' - F')/(F_m' - F_o')$ , which is now commonly referred to as  $F_q'/F_v'$  (Suggett et al. 2003; Baker and Oxborough 2005) or  $qP$  (Kromkamp and Forster 2003). However, our estimate of  $Q_A^{\text{OX}}:Q_A^{\text{TOTAL}}$  (Eq. 2) differs from estimates simply based on measured  $F_q'/F_v'$  with a correction for  $f$ . Specifically, Eq. 2 accounts for the proportion of background fluorescence ( $f$ ) inherent to the absolute fluorescence yield measurements. Two conditions must be met for  $F_o'^{\text{FRR}}$  to equal  $F_o'$ . First, the two FRR chambers must be intercalibrated and thus directly comparable. This condition was met because the FRR enclosed chamber is designed to hold cells over a period of milliseconds to enable relaxation of most photochemical dissipation without significant changes in nonphotochemical dissipation (Falkowski and Kolber 1995). Additionally, the two sampling areas share a common photomultiplier tube for fluorescence detection. We verified that the fluorescence yields from the two FRR chambers were not significantly different when cells were in a completely dark-adapted state before dawn (data not shown). Second, the brief period of time within the FRR enclosed chamber is sufficient to fully relax photochemical but not nonphotochemical dissipatory pathways. This assumption may not always be met because  $Q_A$  reoxidation may be slow in the absence of supplementary far red light, which is not provided by the FASTtracka FRR fluorometer. In addition, some relaxation of nonphotochemical quenching is possible even under brief dark exposure.

Our approach is desirable for in situ productivity determinations because it does not require additional

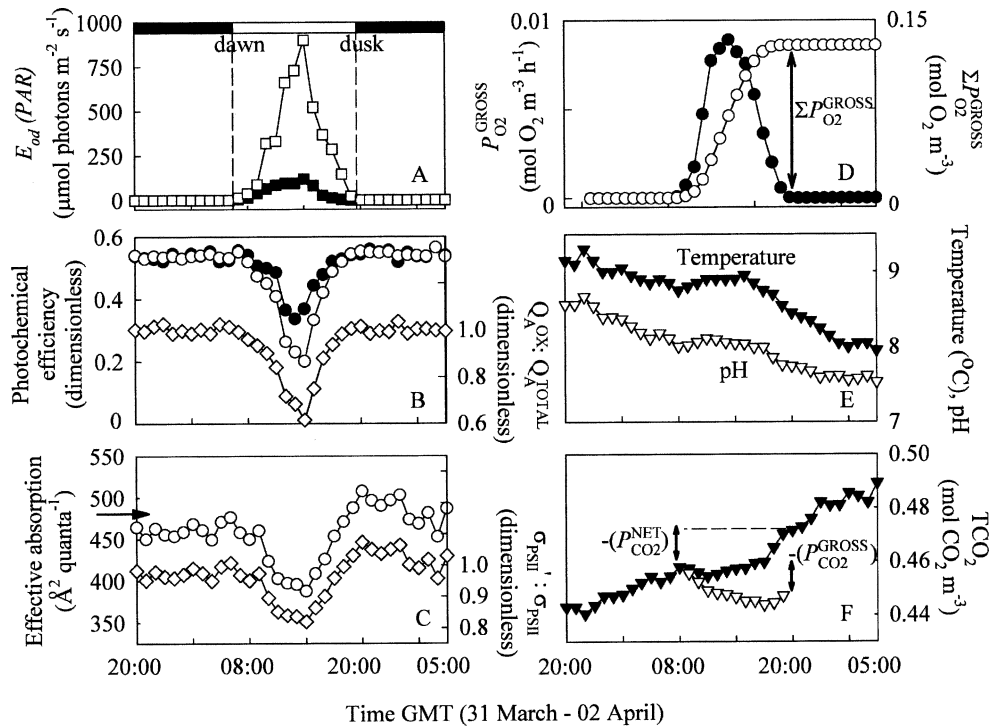


Fig. 2. Diel variability of fluorescence-based and pH-based productivity parameters. (A) Photosynthetically active photon flux density,  $E_{od}(PAR)$  ( $\mu\text{mol photons m}^{-2} \text{s}^{-1}$ ) measured 2 m above water (open squares) and 1 m below the water surface (solid squares). (B) Photochemical efficiency (dimensionless) from the open (open circles) and enclosed (solid circles) FRR chamber, and the proportion of  $Q_a$  that are oxidized ( $Q_a^{OX}:Q_a^{TOTAL}$ , dimensionless), determined as the ratio of photochemical efficiency measured from the open chamber to that from the enclosed chamber (open diamonds) (Eq. 2). (C) Effective absorption, designated  $\sigma_{PSII}'$  during the day and  $\sigma_{PSII}$  at night ( $\text{\AA}^2 \text{ photon}^{-1}$ ) from the FRR enclosed chamber (open circles), and nonphotochemical quenching ( $\sigma_{PSII}':\sigma_{PSII}$ , open diamonds). For calculation of  $\sigma_{PSII}':\sigma_{PSII}$ , the mean from all  $\sigma_{PSII}$  measurements the night before and after each diurnal phase was used (arrow =  $473 \text{\AA}^2 \text{ photon}^{-1}$ ) (see main text). (D) Volume-specific FRR-based gross  $\text{O}_2$  production ( $P_{\text{O}_2}^{\text{GROSS}} = P_{\text{O}_2}^{\text{chl}} \cdot \text{Chl}a$ ) with units of  $\text{mol O}_2 \text{ m}^{-3} \text{ h}^{-1}$  (solid circles), and the cumulative integral of  $P_{\text{O}_2}^{\text{GROSS}}$  throughout the day ( $\text{mol O}_2 \text{ m}^{-3}$ ) (open circles). The sum of  $P_{\text{O}_2}^{\text{GROSS}}$  at the end of the daylight phase is equal to the total daily integrated  $\text{O}_2$  production,  $\Sigma P_{\text{O}_2}^{\text{GROSS}}$ . (E) Temperature ( $^{\circ}\text{C}$ , and pH); (F) Total inorganic carbon ( $\text{TCO}_2$ ,  $\text{mol CO}_2 \text{ m}^{-3}$ ) (solid triangles). The cumulative hourly loss of ( $-$ )  $\text{TCO}_2$  between dawn and dusk is equal to the daily integrated net  $\text{CO}_2$  uptake ( $P_{\text{CO}_2}^{\text{NET}}$ ,  $\text{mol CO}_2 \text{ m}^{-3}$ ). Also shown are  $\text{TCO}_2$  values after correcting for the respiration rate (=daily integrated gross  $\text{CO}_2$  uptake [ $P_{\text{CO}_2}^{\text{GROSS}}$ ,  $\text{mol CO}_2 \text{ m}^{-3}$ ], open triangles). Respiration,  $R$ , was calculated as the mean rate of increase in  $\text{TCO}_2$  from the night before and after each diurnal phase was used (see main text). Note that in this example, net  $\text{CO}_2$  uptake is not observed during daylight hours. Example shown was from 20:00 h GMT 31 March to 05:00 h GMT 02 April 2003.

fully dark-adapted fluorescence measurements that are inherent to some other determinations (Kromkamp and Forster 2003). Furthermore, use of Eq. 2 eliminates the need for a sample blank because values of  $F_m'$  and  $f$  should be identical in the light and dark chambers and thus cancel out. We did not observe any statistical difference between values of  $F_m'$ , as measured directly in situ and thus including  $f$ , from the two FRR chambers during daylight hours throughout the 6-week sampling period (Bartlett's type II regression slope and intercept not significantly different from 1 and 0, respectively,  $p < 0.001$ ,  $n = 441$ , data not shown),

verifying the above assertion. Consequently, variability of  $F_q'/F_v'$ , will be from relative changes in the minimum fluorescence between the two chambers and from absolute changes in maximum fluorescence of both chambers.

Measured values of  $\sigma_{PSII}'$  are weighted to the narrow blue FRR excitation waveband. These were corrected to an effective rate of light absorption for the excitation experienced in situ, termed here as  $\sigma_{PSII}^{\text{abs}}$ . Specifically,  $\sigma_{PSII}'$  was adjusted by using optical absorption coefficients that were spectrally weighted to the incident spectral irradiance,  $E_o$ , of FRR,  $\bar{a}^{\text{chl}}$  (FRR), and in situ,  $\bar{a}^{\text{chl}}$  (in

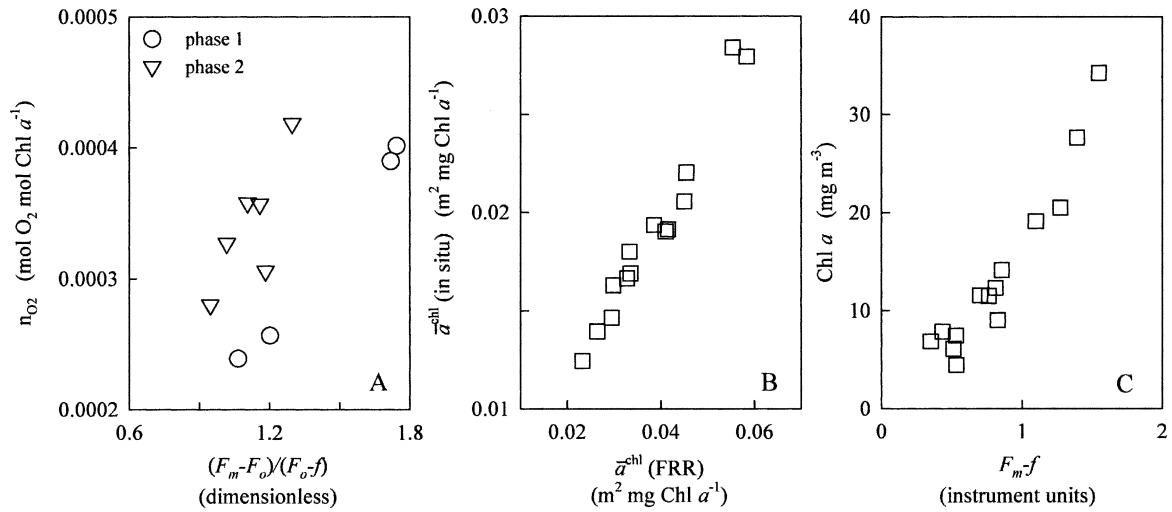


Fig. 3. Comparison of (A) the reciprocal of the Emerson and Arnold number,  $n_{O_2}$  (mol  $O_2$  (mol Chl  $a$ ) $^{-1}$ ), with the blank corrected FRR fluorescence-based “functionality” factor,  $F_v/F_o = (F_m - F_o)/(F_o - f)$  (dimensionless), for all data collected throughout phases 1 and 2. (B) The effective absorption coefficient (Eq. 3) where  $E_o(\lambda)$  is calculated by the in situ ( $\bar{a}^{chl}$  [in situ],  $m^2$  (mg Chl  $a$ ) $^{-1}$ ) versus the FRR fluorometer excitation spectra ( $\bar{a}^{chl}$  [FRR],  $m^2$  (mg Chl  $a$ ) $^{-1}$ ). (C) Chl  $a$  concentration (mg Chl  $a$   $m^{-3}$ ) with the blank-corrected maximum dark-adapted fluorescence yield ( $F_m - f$ , instrument units). Regression equations are given in Table 2.

situ), excitation (Babin et al. 1996; Suggestt et al. 2001; Raateoja et al. 2004),

$$\sigma_{PSII}^{abs'} = \left( \frac{\sigma_{PSII}'}{\bar{a}^{chl}(\text{FRR})} \right) \cdot \bar{a}^{chl}(\text{in situ}) \quad (3)$$

where

$$\bar{a}^{chl} = \left( \sum_{400}^{700} a^{chl}(\lambda) \cdot E_o(\lambda) \right) \Delta\lambda / \sum_{400}^{700} E_o(\lambda) \Delta\lambda$$

Therefore,  $P_{O_2}^{chl}$  (mol  $O_2$  (g Chl  $a$ ) $^{-1}$  h $^{-1}$ ) was finally calculated as

$$P_{O_2}^{chl} = E_{od}(PAR) \cdot \sigma_{PSII}^{abs'} \cdot n_{O_2} \cdot Q_A^{OX} : Q_A^{TOTAL} \cdot 0.0243 \quad (4)$$

Volume-specific daily integrated gross  $O_2$  production,  $\sum P_{O_2}^{GROSS}$  (mol  $O_2$   $m^{-3}$ ), was determined from the product of Chl  $a$  and integral of  $P_{O_2}^{chl}$  throughout the day (Fig. 2D),

$$\sum P_{O_2}^{GROSS} = \left( \sum_{\text{dawn}}^{\text{dusk}} P_{O_2}^{chl}(t) \Delta t \right) \cdot \text{Chl } a \quad (5)$$

where  $t = 1$  h. For the most accurate determination of  $\sum P_{O_2}^{GROSS}$ , daily measurements of  $n_{O_2}$ , spectrally adjusted in situ  $\sigma_{PSII}'$ , and Chl  $a$  concentration must be known. Unfortunately, we could only collect these data every 2–3 d. Therefore, we applied a series of corrections as follows.

First, discrete  $n_{O_2}$  measurements were compared with corresponding in situ FRR fluorescence-based determinations of the factor  $F_v/F_o$ , which can be used to describe the proportion of PSII reaction centers that are functional (Babin et al. 1996) (Fig. 3A).  $n_{O_2}$  was linearly related to the blank-corrected  $F_v/F_o = (F_m - F_o)/(F_o - f)$  for both phase 1 and 2, but followed a different regression equation for each phase (Fig. 3A, Table 2). The high correlation coefficients indicate that  $(F_m - F_o)/(F_o - f)$  is a good descriptor of changes to functional RCII concentration per unit Chl  $a$ . However, the different regression slopes demonstrate that the relationship between  $(F_m - F_o)/(F_o - f)$  and the actual concentrations of RCII per unit Chl  $a$  are not the same for phases 1 and 2 and thus cannot be assumed to be a constant for the entire sampling period. The appropriate linear relationship was applied to the in situ  $(F_m - F_o)/(F_o - f)$  measured daily throughout each of the two phases to derive  $n_{O_2}$ .

Table 2. Regression equations and correlation coefficients for variables compared in Fig. 3. Variables are compared as independent ( $y$ ) versus dependent ( $x$ ). Regression slopes for  $n_{O_2}$  versus the blank corrected functionality factor,  $(F_m - F_o)/(F_o - f)$ , were significantly different between phases 1 and 2,  $t_{v=6}$ : 2.071.

Variables ( $y$ vs. $x$ )	Slope	Intercept	$r^2$	$n$	$p$
$n_{O_2}$ vs. $(F_m - F_o)/(F_o - f)$ (phase 1)	0.00025	-0.00003	0.990	4	<0.05
$n_{O_2}$ vs. $(F_m - F_o)/(F_o - f)$ (phase 2)	0.00034	-0.00001	0.629	6	<0.05
Chl $a$ vs. $F_m - f$	22.46	-4.92	0.905	14	<0.001
$\bar{a}^{chl}$ (in situ) v $\bar{a}^{chl}$ (FRR)	0.467	0.000	0.916	14	<0.001

Second, determinations of  $\bar{a}^{\text{chl}}$  (FRR) and  $\bar{a}^{\text{chl}}$  (in situ) were compared and found to covary according to a single linear relationship throughout the entire sampling period (Fig. 3B, Table 2). The regression from this relationship provided a single correction factor that was applied to each daily measurement of  $\sigma_{\text{PSII}}$  throughout the sampling period.

Third, discrete values of Chl *a* were compared with blank corrected dark-adapted maximum fluorescence yields,  $F_m - f$ , measured from the second bench top FRR fluorometer to develop a regression equation describing the relationship between Chl *a* and the maximum fluorescence yield (Fig. 3C, Table 2). The regression was then applied to estimate Chl *a* from in situ measurements of  $F_m - f$ . Calculation of  $\sum P_{\text{CO}_2}^{\text{GROSS}}$  requires the Chl *a* during the day. However, a true dark-adapted  $F_m$  can be measured only in darkness after nonphotochemical fluorescence quenching has completely relaxed. Therefore, Chl *a* was estimated from the mean  $F_m$  measured the night before and after each diurnal phase.

*In situ pH and estimation of CO<sub>2</sub>*—Water temperature and pH were measured every 15 min at a depth of 1 m using the system described in Maberly (1996) (Fig. 2E). These data, plus weekly measurements of alkalinity (A), were used to calculate the total concentration of inorganic carbon (TCO<sub>2</sub>, mol CO<sub>2</sub> m<sup>-3</sup>, as the sum of free CO<sub>2</sub>, HCO<sub>3</sub><sup>-</sup>, and CO<sub>3</sub><sup>2-</sup>) using the first and second dissociation coefficients corrected for temperature and ionic strength (pK<sub>1</sub>' and pK<sub>2</sub>'), and the calculated concentration of hydroxide ions ([OH<sup>-</sup>]) (Maberly 1996),

$$\text{TCO}_2 = \frac{\left(1 + 10^{(pK_1' - pH)} + 10^{(pH - pK_2')}\right)}{\left(1 + 2\left(10^{(pH - pK_2')}\right)\right)} (A - [\text{OH}^-]) \quad (6)$$

Therefore, TCO<sub>2</sub> was determined at 15-min intervals in the lake. This approach provides a high temporal resolution but has an inherent assumption that changes in TCO<sub>2</sub> result from carbon exchange with the biota rather than, for example, advection of water with high TCO<sub>2</sub> from depth.

*Calculation of net and gross community productivity from diel changes of TCO<sub>2</sub>*—Daily integrated net CO<sub>2</sub> uptake,  $\sum P_{\text{CO}_2}^{\text{NET}}$  (mol CO<sub>2</sub> m<sup>-3</sup>), was determined from the net consumption of the total inorganic carbon concentration, TCO<sub>2</sub>, at 1 m throughout daylight hours (Fig. 2F),

$$\sum P_{\text{CO}_2}^{\text{NET}} = \text{TCO}_2(\text{dusk}) - \text{TCO}_2(\text{dawn}) \quad (7)$$

These  $\sum P_{\text{CO}_2}^{\text{NET}}$  determinations can be affected by vertical mixing events and changes in autotrophic biomass during the day. Therefore, in some circumstances, a diurnal decrease of TCO<sub>2</sub> that is indicative of net CO<sub>2</sub> consumption is not observed (e.g., Fig. 2F).

A community respiration rate (R, mol CO<sub>2</sub> m<sup>-3</sup> h<sup>-1</sup>) was determined to account for the contribution of

autotrophic and heterotrophic respiration. This correction is also affected by environmental fluxes (mixing). R was calculated from the mean rate of increase in TCO<sub>2</sub> throughout each night period (Fig. 2F),

$$R = [\text{TCO}_2(\text{dawn}) - \text{TCO}_2(\text{dusk})] / NL \quad (8)$$

where *NL* is night length between dusk and dawn (h). To account for day-to-day variability in the environment and planktonic community, we used the mean R from the night before and after each diurnal change in TCO<sub>2</sub>. Daily integrated gross CO<sub>2</sub> uptake,  $\sum P_{\text{CO}_2}^{\text{GROSS}}$  (mol CO<sub>2</sub> m<sup>-3</sup>), was determined as

$$\sum P_{\text{CO}_2}^{\text{GROSS}} = \sum P_{\text{CO}_2}^{\text{NET}} + (R \cdot DL) \quad (9)$$

where *DL* is night length between dawn and dusk (h).

## Results and discussion

*Diel variability of FRR photophysiological parameters*—Estimates of daily integrated gross oxygen evolution, designated  $\sum P_{\text{O}_2}^{\text{GROSS}}$ , are driven by the diel patterns of  $E_o$  (*PAR*),  $Q_A^{\text{OX}}:Q_A^{\text{TOTAL}}$ , and  $\sigma_{\text{PSII}}$ , and thus governed by the incident *PAR* in both marine (Gorbunov et al. 2001; Suggett et al. 2001; Moore et al. 2003) and lake (Vincent et al. 1984; Oliver et al. 2003) environments. In Esthwaite Water,  $E_{od}$  (*PAR*) 2 m above water and 1 m below the water were  $966 \pm 46 \mu\text{mol photons m}^{-2} \text{ s}^{-1}$  and  $179 \pm 27.2$  (mean  $\pm$  standard error for all sampling days) at the solar noon maximum, respectively (Fig. 2A). Decreases of  $Q_A^{\text{OX}}:Q_A^{\text{TOTAL}}$  and  $\sigma_{\text{PSII}}$  were also centered on the solar noon (Figs. 2B, C). Daily integrated  $E_{od}$  (*PAR*) above (not shown) and below (Table 3) the water were highest throughout phase 2.

PSII photochemical efficiency under ambient light,  $(F_m' - F') / (F_m' - f)$ , is an estimate of the fraction of absorbed excitation energy used for PSII photochemistry and is lowered by an increase in dissipation (quenching) via photochemical and nonphotochemical pathways. After a brief period of dark acclimation, such as within the enclosed chamber of the FRR fluorometer, the PSII photochemical efficiency can remain lower than dark-adapted values because nonphotochemical but not photochemical dissipation pathways remain active (Kolber and Falkowski 1993; Falkowski and Kolber 1995). Here, the PSII efficiency is strictly defined as the maximum photochemical efficiency under ambient light,  $(F_m' - F_o') / (F_m' - f)$  (Kromkamp and Forster 2003; Suggett et al. 2003) and, as with the calculation of photochemical quenching (Eq. 2), assumes that the minimum fluorescence measured in the FRR enclosed chamber,  $F_o'_{\text{FRR}}$ , is equal to  $F_o'$ . Therefore, variations of PSII photochemical efficiency that are measured in the FRR enclosed chamber will be indicative of changes in the amount of nonphotochemical quenching of excitation energy. From dawn until noon, PSII photochemical efficiency measured in the enclosed chamber decreased by  $34 \pm 5\%$  and  $46 \pm 10\%$  (mean  $\pm$  standard error) for phases 1 and 2, respectively (Figs. 2B, 4).

Table 3. Mean  $\pm$  standard error (minimum–maximum) of variables measured at 1 m throughout phases 1 (28 February–24 March) and 2 (25 March–14 April) of the spring bloom.

Variable	Phase 1	Phase 2
Daily integrated $E_{od}$ ( $PAR$ ) (mol photons $m^{-2}$ )	3.0 $\pm$ 0.5 (1.0–5.8)	5.1 $\pm$ 0.4 (2.1–7.2)
Chl $a$ (mg $m^{-3}$ )	20.1 $\pm$ 4.0 (7.8–34.2)	9.0 $\pm$ 1.7 (4.4–14.1)
$\sigma_{PSII}$ ( $\text{\AA}^2$ photon $^{-1}$ )	360 $\pm$ 14 (303–449)	445 $\pm$ 10 (316–511)
$n_{O_2}$ (mol $O_2$ (mol Chl $a$ ) $^{-1}$ )	3.2 $\cdot$ 10 $^{-4}$ $\pm$ 4.2 $\cdot$ 10 $^{-5}$ (2.3–4.0 $\cdot$ 10 $^{-4}$ )	3.4 $\cdot$ 10 $^{-4}$ $\pm$ 2.0 $\cdot$ 10 $^{-5}$ (2.8–4.4 $\cdot$ 10 $^{-4}$ )
$P_{O_2}^{chl\ MAX}$ (mol $O_2$ (g Chl $a$ ) $^{-1}$ h $^{-1}$ )	0.182 $\pm$ 0.018 (0.121–0.239)	0.258 $\pm$ 0.019 (0.149–0.406)
$\alpha_{PO_2}$ (mol $O_2$ (g Chl $a$ ) $^{-1}$ h $^{-1}$ ) ( $\mu$ mol photons $m^{-2}$ s $^{-1}$ ) $^{-1}$ )	2.2 $\cdot$ 10 $^{-3}$ $\pm$ 1.5 $\cdot$ 10 $^{-4}$ (1.8–2.6 $\cdot$ 10 $^{-3}$ )	2.9 $\cdot$ 10 $^{-3}$ $\pm$ 2.0 $\cdot$ 10 $^{-4}$ (2.0–3.4 $\cdot$ 10 $^{-3}$ )
Predominant species (% cells)	<i>Asterionella formosa</i> (93%) <i>Anabaena circinalis</i> (4%) <i>Cyclotella</i> spp. (2%)	<i>Asterionella formosa</i> (55%) <i>Anabaena circinalis</i> (17%) <i>Rhodomonas</i> spp. (13%) <i>Chrysochromulina parva</i> (11%)

Variables shown are daily integrated  $E_{od}$  ( $PAR$ ) (mol photons  $m^{-2}$ ), Chl  $a$  concentration (mg  $m^{-3}$ ), mean dark-adapted effective absorption ( $\sigma_{PSII}$ ,  $\text{\AA}^2$  photon $^{-1}$ ), reciprocal of the Emerson and Arnold number ( $n_{O_2}$ , mol  $O_2$  (mol Chl  $a$ ) $^{-1}$ ), and the maximum rate and initial slope of FRR-based Chl  $a$ -normalized  $O_2$  production,  $P_{O_2}^{chl\ MAX}$  (mol  $O_2$  (g Chl  $a$ ) $^{-1}$  h $^{-1}$ ) and  $\alpha_{PO_2}$  ((mol  $O_2$  (g Chl  $a$ ) $^{-1}$  h $^{-1}$ )( $\mu$ mol photons  $m^{-2}$  s $^{-1}$ ) $^{-1}$ ), respectively.  $P_{O_2}^{chl\ MAX}$  and  $\alpha_{PO_2}$  were determined from each daily light-response of  $P_{O_2}^{chl}$  in situ by least-squares nonlinear regression to the equation of Jassby and Platt (1976),  $P_{O_2}^{chl} = P_{O_2}^{chl\ MAX} \cdot (1 - \exp(-\alpha_{PO_2} \cdot PPF)) / P_{O_2}^{chl\ MAX}$ . Data were only used where  $P_{O_2}^{chl}$  was clearly saturated with respect to the  $E_{od}$  ( $PAR$ ). This criterion provided  $n = 7$  and 16 from the 13 and 21 d of daily  $P_{O_2}^{chl}$  versus  $E_{od}$  ( $PAR$ ) at 1 m from throughout phases 1 and 2, respectively. Each variable was significantly different between phases 1 and 2 ( $t$  test with unequal sample sizes; data not shown). Microscopy measurements shown for phases 1 and 2 were determined from 18 March and 01 April, respectively.

The effective absorption cross section measured at steady state (i.e., phytoplankton acclimated to ambient light),  $\sigma_{PSII}'$ , reflects the size of the light harvesting antenna and is reduced with increased energy dissipation via nonphotochemical quenching in the antenna bed. Therefore, we used a second approach to determine the extent of nonphotochemical quenching as the decrease in effective absorption between dawn and noon ( $=\sigma_{PSII}':\sigma_{PSII}$ , Fig. 2C). The main drawback of this second approach is that the effective absorption can also change as a result of photoacclimatory and inhibitory driven alterations to the light-harvesting pigment beds and reaction center complexes (Suggett et al. 2004). Therefore, mean  $\sigma_{PSII}$  measurements from the night before and after each diurnal phase were used to account for this possible source of error from day to day (Fig. 2C).  $\sigma_{PSII}'$  decreased relative to  $\sigma_{PSII}$  by 22  $\pm$  5% and 28  $\pm$  12% between dawn and solar noon for phases 1 and 2, respectively (Figs. 2C, 4).

In contrast to the effective absorption cross section, the PSII photochemical efficiency is indicative of nonphotochemical dissipation that occurs within both the antennae bed and the PSII reaction centers (Gorbunov et al. 2001). Nonphotochemical dissipation estimated from decreases of  $(F_m' - F_o'_{FRR})/(F_m' - f)$  between dawn and noon was greater than that determined from decreases of effective absorption cross section by  $\sim$ 0 and 50% (Fig. 4) but on average by 21% and 25% for phases 1 and 2, respectively. Given the assumptions above, this percentage suggests a relatively small amount of PSII reaction center-based quenching occurred in these phytoplankton communities and thus that the majority of RCIIIs remained functional throughout.

**Photosynthetic unit size**—Strong correlations between  $n_{O_2}$  and measured  $F_v/F_o$ ,  $(F_m - F_o)/(F_o - f)$  for phases 1 and 2 (Table 2, Fig. 3A) suggest that changes in  $n_{O_2}$  occur partly from modifications to the proportion of RCIIIs that are active (Babin et al. 1996).  $F_v/F_o$  changed by  $\sim$ 20–30% throughout the investigation, a magnitude that was consistent with the average amount of PSII reaction center-based quenching observed throughout phases 1 (21%) and 2 (25%) (above, Fig. 4).

Previous FRR fluorescence-based estimates of  $P_{O_2}^{chl}$  have used “typical”  $n_{O_2}$  values of 5.0  $\cdot$ 10 $^{-4}$  and 1.0 $\cdot$ 10 $^{-3}$  mol  $O_2$  (mol Chl  $a$ ) $^{-1}$  for eukaryotic phytoplankton and cyanobacteria, respectively, based on data from laboratory experiments of few isolates (Moore et al. 2003; Raateoja et al. 2004; Smyth et al. 2004). To estimate the actual  $n_{O_2}$  yield from active RCIIIs per unit Chl  $a$ , the “typical”  $n_{O_2}$  is then multiplied by  $F_v/F_o$  normalized to a theoretical maximum ( $\approx$ an  $F_v/F_o$  of 1.8; Babin et al. 1996). Our measured values of  $n_{O_2}$  for natural lake communities were 3.2 and 3.4 $\cdot$ 10 $^{-4}$  mol  $O_2$  (mol Chl  $a$ ) $^{-1}$  for phases 1 and 2 (Table 3). These values are  $\sim$ 20% lower and 10% higher (respectively) than using the product of the “typical” value of 5.0  $\cdot$ 10 $^{-4}$  mol  $O_2$  (mol Chl  $a$ ) $^{-1}$  and the factor  $[F_v/F_o]/1.8$  (data not shown) when direct measurements are not available. Therefore, and in agreement with observations by Suggett et al. (2004), this alternative approach can yield an estimate of  $O_2$  evolved by active RCIIIs (Chl  $a$ ) $^{-1}$  with considerable error, most likely from assumed values of the “typical”  $n_{O_2}$  and the theoretical maximum for  $F_v/F_o$ . Our measurements of  $n_{O_2}$  here are consistent with laboratory data for eukaryotic phytoplankton species under nutrient replete conditions (see Suggett et al. 2004).

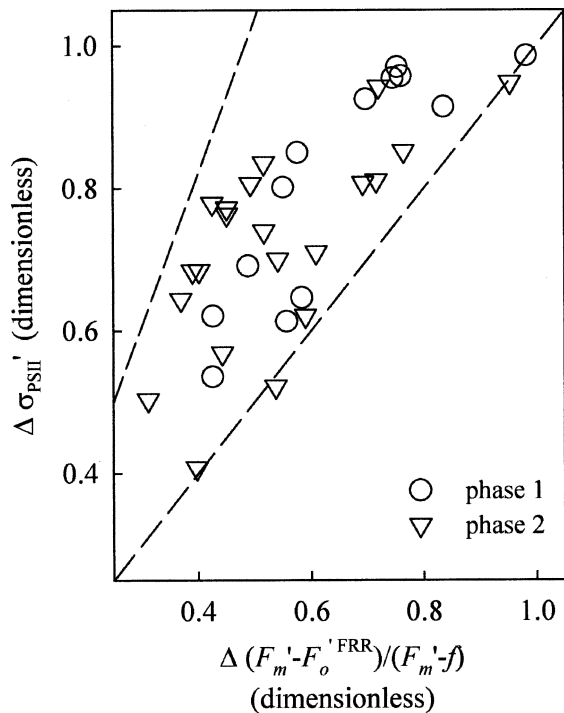


Fig. 4. Extent of nonphotochemical quenching determined as the ratio of maximum photochemical efficiency or effective absorption at noon to that at dawn for each day of sampling,  $\Delta(F_m' - F_o'^{FRR})/(F_m' - f)$  and  $\Delta\sigma_{PSII}'$ , respectively. Here,  $(F_m' - F_o'^{FRR})/(F_m' - f)$  and  $\sigma_{PSII}'$  at dawn is equal to the blank corrected maximum PSII photochemical efficiency under dark adaptation,  $(F_m - F_o)/(F_m - f)$  and the maximum PSII effective absorption cross section under dark adaptation,  $\sigma_{PSII}$ . However, for simplicity, we have termed the ratio of either parameter between noon and dawn as  $\Delta$ . Day-to-day photoacclimatory and photoinhibitory driven variances in  $\sigma_{PSII}$  are accounted for as described in the main text. All fluorescence parameters were taken from the FRR enclosed chamber. Dashed lines indicate  $\Delta(F_m' - F_o'^{FRR})/(F_m' - f)$ :  $\Delta\sigma_{PSII}'$  limits of 1:1 and 1:2. For points that fall on the 1:1 line, all of the nonphotochemical quenching can be attributed to the change in the effective cross section and thus to quenching that takes place in the pigment bed. For points that fall above the 1:1 line, we infer that a proportion of the nonphotochemical quenching occurs in the reaction centers.

**Community respiration**—Nocturnal respiration rates of  $CO_2$  (R) were  $37 \pm 28\%$  (mean  $\pm$  standard deviation) and  $130 \pm 107\%$  of the mean diurnal net  $CO_2$  uptake rates for phases 1 and 2, respectively. Daily integrated gross  $CO_2$  uptake,  $\sum P_{CO_2}^{GROSS}$ , was determined as the sum of  $\sum P_{CO_2}^{NET}$  and R (Eq. 9, Fig. 2F). Respiration rates, and hence the difference between net and gross  $CO_2$  uptake, was greater for phase 2 than phase 1 (Table 4). Phase 1 was characterized by higher phytoplankton biomass than phase 2 (see Chl *a*, Table 3). As such, our results are consistent with enhanced heterotrophy:autotrophy under conditions of lower phytoplankton biomass (del Giorgio et al. 1999) and a possible increase in grazing pressure. The differences in R may also partly reflect changes in the planktonic community assemblage. However, in our calculation of gross  $CO_2$  uptake we must assume that heterotrophic

activity and hence respiration (R) is equal during the day and night (Cole et al. 2000). In addition, the respiration term will also account for day-night differences in  $TCO_2$  from environmental fluxes, for example, enhanced nocturnal mixing leading to diel patterns in stratification and from autotrophic respiration. Consequently, it is arguable that the actual in situ  $TCO_2$  uptake lies somewhere between the estimates with and without the inclusion of R.

**Comparing FRR fluorescence- and  $TCO_2$ -based productivity**—Daily integrated net  $CO_2$  uptake,  $\sum P_{CO_2}^{NET}$ , was linearly correlated with daily integrated gross oxygen evolution,  $\sum P_{O_2}^{GROSS}$ , during both phases: 85% and 67% of the variance in  $\sum P_{CO_2}^{NET}$  could be attributed to a linear dependence on  $\sum P_{O_2}^{GROSS}$  in phases 1 and 2, respectively (Table 4).  $\sum P_{CO_2}^{NET}$  was  $53 \pm 10\%$  (mean  $\pm$  standard error) and  $26 \pm 9\%$  of  $\sum P_{O_2}^{GROSS}$  for phases 1 and 2, respectively (Table 4, Fig. 5A). Note that for some days,  $\sum P_{CO_2}^{NET}$  was negative (Fig. 5A), thus indicating a net flux of  $TCO_2$  from the water column. These days corresponded with high wind speeds during phase 1 and a breakdown in water column stratification during phase 2 (data not shown). Hence accounting for the daily respiration term, R, was essential for comparing  $O_2$  production and  $CO_2$  uptake for the entire data set.

Daily gross  $CO_2$  uptake,  $\sum P_{CO_2}^{GROSS}$ , was strongly linearly correlated with, but systematically lower than,  $\sum P_{O_2}^{GROSS}$  (Table 4). The mean ( $\pm$  standard error) of  $\sum P_{O_2}^{GROSS}$ :  $\sum P_{CO_2}^{GROSS}$  was  $1.01 \pm 0.04$  for phase 1 and  $1.53 \pm 0.13$  for phase 2 (Table 4, Fig. 5B). Thus, the photosynthetic quotient relating FRR-based estimates of  $O_2$  evolved with gross community carbon assimilated was higher throughout phase 2.

There was relatively little day-to-day variability in the relationship between gross  $CO_2$  uptake and gross FRR-based  $O_2$  evolution; only  $\sim 10$ – $25\%$  of the variance in  $\sum P_{CO_2}^{GROSS}$  could not be explained by the linear regression on  $\sum P_{O_2}^{GROSS}$  (Table 4, Fig. 5). This provides strong evidence of a systematic coupling between photosynthetic electron transfer and  $CO_2$  fixation for the phytoplankton communities during both phases 1 and 2. However, two of the main determinants of  $\sum P_{O_2}^{GROSS}$ ,  $E_{od}$  (PAR) and phytoplankton biomass, also varied significantly throughout phases 1 and 2 (Table 3). Therefore, it is possible that variations of gross  $CO_2$  uptake,  $\sum P_{CO_2}^{GROSS}$ , may be accounted for by the daily integrated  $E_{od}$  (PAR),  $\Sigma E_{od}$  (PAR), and Chl *a* without recourse to calculate  $\sum P_{O_2}^{GROSS}$ .

The product of  $\Sigma E_{od}$  (PAR) and Chl *a* accounted for 27 to 42% of the variability in  $\sum P_{CO_2}^{GROSS}$  (Fig. 5C, Table 4). This is  $\sim 30$ – $50\%$  lower than the amount of variability in  $\sum P_{CO_2}^{GROSS}$  that can be attributed to  $\sum P_{O_2}^{GROSS}$  (Table 4). In addition, the extent of variability of both  $\Sigma E_{od}$  (PAR) and Chl *a* (the standard error was approximately  $\pm 25\%$  of the mean) exceeded that observed for parameters describing light absorption (standard error approximately  $\pm 5$ – $10\%$  of the mean) (Table 3). However, greater than 50% of sampling days demonstrated that  $P_{O_2}^{chl}$  was saturated with

Table 4. Bartlett type II regression equations and correlation coefficients for data compared in Fig. 5. Variables are compared as independent ( $y$ ) versus dependent ( $x$ ). Regressions for daily net CO<sub>2</sub> uptake ( $\sum P_{\text{CO}_2}^{\text{NET}}$ ) versus daily gross O<sub>2</sub> evolution ( $P_{\text{O}_2}^{\text{GROSS}}$ ) exclude data where  $\sum P_{\text{CO}_2}^{\text{NET}}$  is negative (see Fig. 5A). Regression slopes for  $\sum P_{\text{CO}_2}^{\text{NET}}$  and daily gross CO<sub>2</sub> uptake ( $\sum P_{\text{CO}_2}^{\text{GROSS}}$ ) versus  $\sum P_{\text{O}_2}^{\text{GROSS}}$  and for  $\sum P_{\text{CO}_2}^{\text{GROSS}}$  versus  $\sum E_{\text{od}}(\text{PAR}) \cdot \text{Chl } a$  were significantly different ( $p < 0.05$ ) between phases 1 and 2,  $t_v = 25:2.345$  and  $t_v = 30:3.583$ , respectively.

Phase	Variables ( $y$ vs. $x$ )	Slope	Intercept	$r^2$	$n$	$p$
1	Daily net CO <sub>2</sub> uptake vs. $\sum P_{\text{O}_2}^{\text{GROSS}}$	0.828	-0.0026	0.845	12	<0.001
	Daily gross CO <sub>2</sub> uptake vs. $\sum P_{\text{O}_2}^{\text{GROSS}}$	0.981	0.0001	0.805	13	<0.001
	Daily gross CO <sub>2</sub> uptake vs. $\sum E_{\text{od}}(\text{PAR}) \text{Chl } a$	0.394	-0.0020	0.267	13	<0.001
2	Daily net CO <sub>2</sub> uptake vs. $\sum P_{\text{O}_2}^{\text{GROSS}}$	0.481	0.0009	0.667	17	<0.001
	Daily gross CO <sub>2</sub> uptake vs. $\sum P_{\text{O}_2}^{\text{GROSS}}$	0.644	0.0010	0.728	21	<0.001
	Daily gross CO <sub>2</sub> uptake vs. $\sum E_{\text{od}}(\text{PAR}) \text{Chl } a$	0.229	-0.0001	0.419	21	<0.001

respect to  $E_{\text{od}}(\text{PAR})$  (see Table 3). Consequently, evidence suggests that biomass and light cannot exclusively account for the variability of production that was observed. Also, that variability of the light-response characteristics of  $\sum P_{\text{O}_2}^{\text{GROSS}}$ , as quantified by FRR, and of the coupling between gross O<sub>2</sub> evolution and CO<sub>2</sub> assimilation must significantly account for the variability of community metabolism.

The higher photosynthetic quotient for phase 2 was associated with a systematic alteration in the phytoplankton community structure and the lake environment (Table 3). Phase 1 was characterized by a diatom dominated assemblage (Table 3) and relatively high nutrient concentrations (data not shown). Phase 2 was characterized by significantly higher numbers of flagellates, *Rhodomonas*

spp. and *Chrysochromulina parva*, and the cyanobacterium *Anabaena circinalis*. This change in the phytoplankton assemblage between phase 1 and 2 was consistent with previous changes that have followed an exhaustion of silicate and rapid stabilization of the water column (Maberly et al. 1994). The differences in the PQ are consistent with observations from unialgal cultures of diatoms and cryptophytes (MacIntyre et al. unpubl. data). Specifically, MacIntyre et al. (unpubl. data) found that the diatom *Thalassiosira weissflogii* displays lower photosynthetic quotients of ( $\sim 1.5 \text{ mol O}_2 (\text{mol CO}_2)^{-1}$ ) than the cryptophyte *Streatula major* ( $\sim 2.5 \text{ mol O}_2 (\text{mol CO}_2)^{-1}$ ) under nutrient replete growth conditions. Thus, the direction and magnitude of the change that we observed in Esthwaite Water is consistent with observations from unialgal cultures. Specific reasons for these taxonomic

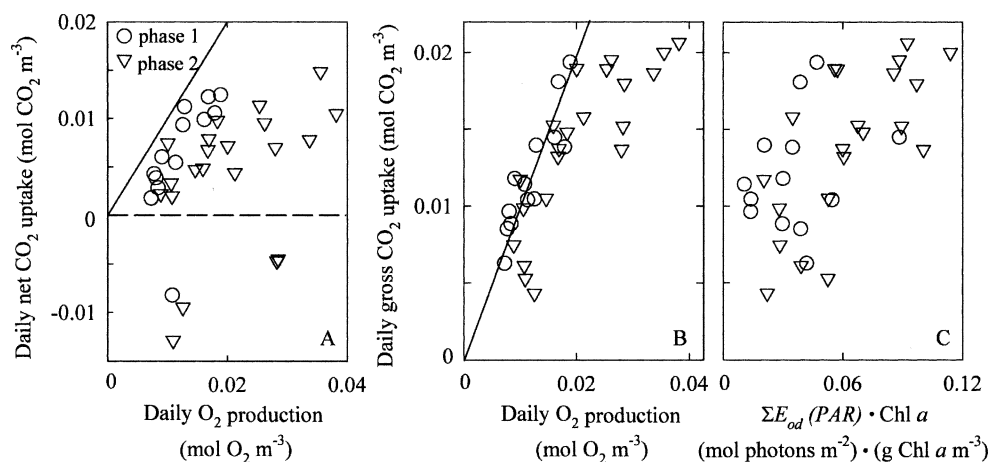


Fig. 5. Comparison of pH-based daily integrated (A) net CO<sub>2</sub> uptake ( $\sum P_{\text{CO}_2}^{\text{NET}}$ , mol CO<sub>2</sub> m<sup>-3</sup>) and (B) gross CO<sub>2</sub> uptake ( $\sum P_{\text{CO}_2}^{\text{GROSS}}$ , mol CO<sub>2</sub> m<sup>-3</sup>) with FRR fluorescence-based daily integrated O<sub>2</sub> production ( $\sum P_{\text{O}_2}^{\text{GROSS}}$ , mol O<sub>2</sub> m<sup>-3</sup>). The solid diagonal line indicates a photosynthetic quotient of  $P_{\text{O}_2}^{\text{GROSS}}$  per unit CO<sub>2</sub> uptake of 1. (C)  $\sum P_{\text{CO}_2}^{\text{GROSS}}$  with the product of daily integrated  $E_{\text{od}}(\text{PAR})$  (mol photons m<sup>-2</sup>) and Chl  $a$  concentration (g Chl  $a$  m<sup>-3</sup>). Regression equations are given in Table 4.

differences in the photosynthetic quotient are not clear but presumably represent distinct photosynthetic architectures of different higher taxonomic groupings.

Three processes may explain the differences observed between  $\sum P_{O_2}^{GROSS}$  and  $\sum P_{CO_2}^{GROSS}$  (Prášil et al. 1996; Geider and MacIntyre 2002; Wilhelm et al. 2004): (1) electron sinks within the photosynthetic electron transfer chain, (2) photorespiratory  $O_2$  consumption, and (3) consumption of NADPH by essential photochemical processes other than  $CO_2$  fixation, such as nitrate reduction and assimilation. These pathways will be briefly discussed.

Two electron cycling pathways contribute to turnover of PSII, and hence FRR estimates of gross oxygen evolution, without net  $O_2$  evolution and thus without net  $CO_2$  fixation. First, cycling of electrons around PSII may occur under high light (Falkowski et al. 1988; Prášil et al. 1996). These authors suggested that cycling of electrons around PSII may account up to ~30% of the PSII linear electron flow under exposure to light-saturated irradiances for cultures of *Chlorella* sp. and *Chaetoceros gracilis*. Second, oxygen may be reduced at PSI by the Mehler reaction (Kana 1992). These processes increase the minimum quantum requirement for the evolution of 1 mol  $O_2$  (Falkowski et al. 1988; Prášil et al. 1996; Noctor and Foyer 1998). Lewitus and Kana (1995) estimated that the Mehler reaction can account for up to ~50% of light-saturated gross  $O_2$  evolution for isolates of eukaryotic estuarine phytoplankton species *Pavlova* sp., *Closterium* sp., *Cryptomonas* sp., and *Hemiselmis* sp. Our measurements of  $P_{O_2}^{chl}$  were saturated with respect to  $E_{od}$  (PAR), suggesting a possible contribution of these two electron cycling pathways to  $P_{O_2}^{chl}$ , for more than 50% of sampling days (see Table 3).

Photorespiration may also consume a proportion of the  $O_2$  evolved during linear electron transfer (Badger et al. 2000; Ort and Baker 2002) where  $O_2$  successfully outcompetes  $CO_2$  for ribulose 1,5-bisphosphate (RuBP) at the active site of RUBISCO. In this case, gross  $CO_2$  assimilation but not linear electron transfer (or gross  $O_2$  evolution) will decrease to yield a photosynthetic quotient for the ratio of oxygen evolution to net carbon dioxide fixation that is lower than we calculate from  $\sum P_{O_2}^{GROSS} : \sum P_{CO_2}^{GROSS}$ . Photorespiration is stimulated when there is relatively low inorganic carbon availability (Geider and MacIntyre 2002). However, it is unlikely that photorespiration was significant because the lake pH remained relatively low throughout the investigation (data not shown). Furthermore, addition of  $NaHCO_3$  did not alter  $n_{O_2}$  measurements (data not shown).

NADPH produced from linear electron flow ( $\sum P_{O_2}^{GROSS}$ ) will be allocated between  $CO_2$  fixation and other energy-demanding photosynthetic processes, for example, nitrate and sulphate reduction and reductive biosynthesis, such as lipid biosynthesis. Consequently, this allocation is reflected in the stoichiometry for phytoplankton growth (Falkowski and Raven 1997; Geider and MacIntyre 2002). Nitrate assimilation requires a higher ratio of gross oxygen evolution to carbon fixation than ammonium assimilation

(Laws 1991). The ratio of ammonium to nitrate was higher during phase 2 than phase 1 as a result of both lower nitrate and higher ammonium concentrations (data not shown). Therefore, we might expect the photosynthetic quotient to be lower in phase 2. Contrary to this expectation, we found a higher photosynthetic quotient during phase 2. Despite the changes in inorganic nitrogen concentrations between phases 1 and 2, we do not have evidence to suggest nitrate concentrations became limiting for microalgal growth or that ammonia became the main source of nitrogen during phase 2.

We have demonstrated a tight coupling between daily photosynthetic electron transfer rate (e.g., potential  $O_2$  production) and daily gross  $CO_2$  uptake in situ. Our results strongly indicate that the community metabolism in Esthwaite Water during the spring bloom was driven by gross phytoplankton photosynthesis. Furthermore, the ratio of light absorption to inorganic carbon fixation depends on the taxonomic makeup of the phytoplankton community.

Our investigation provides further confidence in the use of the FRR technique as a measure of primary productivity in situ. Several investigations have previously used FRR fluorometry to assess microalgal productivity in situ (Suggett et al. 2001; Raateoja et al. 2004; Smyth et al. 2004) but have been limited by assuming  $n_{O_2}$  and lack of knowledge of the fluorescence blank relative to the sample (Cullen and Davis 2003). Furthermore, implementation of FRR fluorescence as a tool for directly measuring "productivity" is fraught with difficulty where photosynthetic pathways uncouple absorbed light, linear electron flow, and reductant partitioning from assimilated carbon (Kromkamp and Forster 2003; Suggett et al. 2004; Wilhelm et al. 2004). We have demonstrated an FRR approach that overcomes uncertainties inherent to these previous  $P_{O_2}^{chl}$  determinations.  $\sum P_{O_2}^{GROSS}$  and  $\sum P_{CO_2}^{GROSS}$  were tightly coupled for these spring bloom phytoplankton communities exhibiting little RCII damage (20–30%) and hence RCII-based fluorescence quenching. There will no doubt be conditions in which  $P_{O_2}^{GROSS}$  diverges from  $\sum P_{CO_2}^{GROSS}$ , such as an unfavorable growth environment and/or a change in phytoplankton community. However, experimental programs that combine both biophysical (FRR) and gas exchange (diel pH and diel  $O_2$ ) measurements hold promise for gaining significant insights into the role of phytoplankton photophysiology in phytoplankton ecology.

## References

- BABIN, M., A. MOREL, H. CLAUSTRE, C. BRICAUD, Z. KOLBER, AND P. G. FALKOWSKI. 1996. Nitrogen- and irradiance-dependent variations of the maximum quantum yield of carbon fixation in eutrophic, mesotrophic and oligotrophic marine systems. *Deep-Sea Res. I* **43**: 1241–1272.
- BADGER, M. R., S. VON CAEMMERER, S. RUUSKA, AND H. NAKANO. 2000. Electron flow to oxygen in higher plants and algae: rates and control of direct photoreduction (Mehler reaction) and rubisco oxygenase. *Phil. Trans. Royal Soc. B* **355**: 1433–1446.

- BAKER, N. R., AND K. OXBOROUGH. 2005. Chlorophyll *a* fluorescence as a probe of photosynthetic productivity, p. 65–82. In G. C. Papageorgiou and Govindjee [eds.], Chlorophyll *a* fluorescence: A signature of photosynthesis. Springer.
- BARLOW, R. G., D. G. CUMMINGS, AND S. W. GIBB. 1997. Improved resolution of mono- and divinyl chlorophylls *a* and *b* and zeaxanthin and lutein in phytoplankton using reverse phase C-8 HPLC. *Mar. Ecol. Prog. Ser.* **161**: 303–307.
- CLEVELAND, J. S., AND A. D. WIEDEMANN. 1993. Quantifying absorption by aquatic particles: A multiple scattering correction for glass-fibre filters. *Limnol. Oceanogr.* **38**: 1321–1327.
- COLE, J. J., M. L. PACE, S. R. CARPENTER, AND J. F. KITCHELL. 2000. Persistence of net heterotrophy in lakes during nutrient addition and food web manipulations. *Limnol. Oceanogr.* **45**: 1718–1730.
- CULLEN, J. J., AND R. F. DAVIS. 2003. The blank can make a big difference in oceanographic measurements. *Limnol. Oceanogr. Bull.* **12**: 29–35.
- DEL GIORGIO, P. A., J. J. COLE, N. F. CARACO, AND R. H. PETERS. 1999. Linking planktonic biomass and metabolism to net gas fluxes in northern temperate lakes. *Ecology* **80**: 1422–1431.
- FALKOWSKI, P. G., AND Z. S. KOLBER. 1995. Variations in chlorophyll fluorescence yields in phytoplankton in the world's oceans. *Austr. J. Plant Physiol.* **22**: 341–355.
- , ———, AND Y. FUJITA. 1988. Effect of redox state on the dynamics of photosystem II during steady state fluorescence in eucaryotic algae. *Biochim. Biophys. Acta* **933**: 432–443.
- , AND J. A. RAVEN. 1997. Aquatic photosynthesis. Blackwell Science.
- FERRARI, G. M., AND S. TASSAN. 1999. A method for removal of light absorption by phytoplankton pigments using chemical oxidation. *J. Phycol.* **35**: 1090–1098.
- GEIDER, R. J., AND H. L. MACINTYRE. 2002. Physiology and biochemistry of photosynthesis and algal carbon acquisition, p. 44–77. In P. J. le B. Williams, D. N. Thomas, and C. S. Reynolds [eds.], Phytoplankton productivity: Carbon assimilation in marine and freshwater ecosystems. Blackwell Science.
- GELDA, R. K., AND S. W. EFFLER. 2002. Metabolic rate estimates for a eutrophic lake from diel dissolved oxygen signals. *Hydrobiologia* **485**: 51–66.
- GORBUNOV, M. Y., Z. S. KOLBER, M. P. LESSER, AND P. G. FALKOWSKI. 2001. Photosynthesis and photoprotection in symbiotic corals. *Limnol. Oceanogr.* **46**: 75–85.
- JASSBY, A. T., AND T. PLATT. 1976. Mathematical formulation of the relationship between photosynthesis and light for phytoplankton. *Limnol. Oceanogr.* **21**: 540–547.
- KANA, T. M. 1992. Relationship between photosynthetic oxygen cycling and carbon assimilation in *Synechococcus* WH7803 (Cyanophyta). *J. Phycol.* **28**: 304–308.
- KIRK, J. T. O. 1994. Light and photosynthesis in aquatic ecosystems. Cambridge Univ. Press.
- KOLBER, Z. S., AND P. G. FALKOWSKI. 1993. Use of active fluorescence to estimate phytoplankton photosynthesis in situ. *Limnol. Oceanogr.* **38**: 1646–1665.
- , O. PRÁŠIL, AND P. G. FALKOWSKI. 1998. Measurements of variable chlorophyll fluorescence using fast repetition rate techniques: Defining methodology and experimental protocols. *Biochim. Biophys. Acta* **1367**: 88–106.
- KROMKAMP, J. C., AND R. M. FORSTER. 2003. The use of variable fluorescence measurements in aquatic ecosystems: Differences between multiple and single turnover measuring protocols and suggested terminology. *Eur. J. Phycol.* **38**: 103–112.
- LANEY, S. R. 2003. Assessing the error in photosynthetic properties determined by fast repetition rate fluorometry. *Limnol. Oceanogr.* **48**: 2234–2242.
- LAWS, E. 1991. Photosynthetic quotients, new production and net community production in the open ocean. *Deep-Sea Res.* **38**: 143–167.
- LEWITUS, A. J., AND T. M. KANA. 1995. Light respiration in six estuarine phytoplankton species: Contrasts under photoautotrophic and mixotrophic growth conditions. *J. Phycol.* **31**: 754–761.
- LUND, J. W. G. 1962. Concerning a counting chamber for nanoplankton described previously. *Limnol. Oceanogr.* **7**: 261–262.
- MABERLY, S. C. 1996. Diel, episodic and seasonal changes in pH and concentrations of inorganic carbon in a productive lake. *Freshwater Biol.* **35**: 579–598.
- , M. A. HURLEY, C. BUTTERWICK, J. E. CORRY, S. I. HEANEY, A. E. IRISH, G. H. M. JAWORSKI, J. W. G. LIND, C. S. REYNOLDS, AND J. Y. ROSCOE. 1994. The rise and fall of *Asterionella formosa* in the southern basin of Windermere: Analysis of a 45-year series of data. *Freshwater Biol.* **31**: 19–34.
- MOORE, C. M., M. I. LUCAS, R. SANDERS, AND R. DAVIDSON. 2005. Basin-scale variability of phytoplankton bio-optical characteristics in relation to bloom state and community structure in the Northeast Atlantic. *Deep-Sea Res.* **52**: 401–419.
- , D. J. SUGGETT, P. M. HOLLIGAN, J. SHARPLES, E. R. ABRAHAM, M. I. LUCAS, T. P. RIPPETH, N. R. FISHER, J. H. SIMPSON, AND D. J. HYDES. 2003. Physical controls on phytoplankton physiology and production at a shelf sea front: A fast repetition rate fluorometer based field study. *Mar. Ecol. Prog. Ser.* **259**: 29–45.
- NOCTOR, G., AND C. H. FOYER. 1998. A re-evaluation of the ATP: NADPH budget during C<sub>3</sub> photosynthesis: A contribution from nitrate assimilation and its associated respiratory activity? *J. Exp. Bot.* **49**: 1895–1908.
- OLIVER, R. L., J. WHITTINGTON, Z. LOHRENZ, AND I. T. WEBSTER. 2003. The influence of vertical mixing on the photoinhibition of variable chlorophyll *a* fluorescence and its inclusion in a model of phytoplankton photosynthesis. *J. Plankton Res.* **25**: 1107–1129.
- ORT, D. R., AND N. R. BAKER. 2002. A photoprotective role for O<sub>2</sub> as an alternative electron sink in photosynthesis? *Curr. Opin. Plant Biol.* **5**: 193–198.
- PRÁŠIL, O., Z. KOLBER, J. A. BERRY, AND P. G. FALKOWSKI. 1996. Cyclic electron flow around photosystem II in vivo. *Photosynth. Res.* **48**: 395–410.
- RAATEOJA, M., J. SEPPÄLÄ, AND H. KUOSA. 2004. Bio-optical modelling of primary production in the SW Finnish coastal zone, Baltic Sea: Fast repetition rate fluorometry in Case 2 waters. *Mar. Ecol. Prog. Ser.* **267**: 9–26.
- SMYTH, T. J., K. L. PEMBERTON, J. AIKEN, AND R. J. GEIDER. 2004. A methodology to determine primary production and phytoplankton photosynthetic parameters from fast repetition rate fluorometry. *J. Plankton Res.* **26**: 1337–1350.
- SUGGETT, D., G. KRAAY, P. HOLLIGAN, M. DAVEY, J. AIKEN, AND R. GEIDER. 2001. Assessment of photosynthesis in a spring cyanobacterial bloom by use of a fast repetition rate fluorometer. *Limnol. Oceanogr.* **46**: 802–810.
- , H. L. MACINTYRE, AND R. J. GEIDER. 2004. Evaluation of biophysical and optical determinations of light absorption by photosystem II in phytoplankton. *Limnol. Oceanogr. Methods* **2**: 316–332.

- , K. OXBOROUGH, N. R. BAKER, H. L. MACINTYRE, T. M. KANA, AND R. J. GEIDER. 2003. Fast repetition rate and pulse amplitude modulation chlorophyll *a* fluorescence measurements for assessment of photosynthetic electron transport in marine phytoplankton. *Eur. J. Phycol.* **38**: 371–384.
- VINCENT, W. F., P. J. NEALE, AND P. J. RICHERSON. 1984. Photoinhibition: Algal responses to bright light during diel stratification and mixing in a tropical alpine lake. *J. Phycol.* **20**: 201–211.
- WILHELM, C., A. BECKER, J. TOEPEL, A. VIELER, AND R. RAUTENBERGER. 2004. Photophysiology and primary production of phytoplankton in freshwater. *Physiol. Plantarum* **120**: 347–357.

*Received: 6 February 2006*

*Accepted: 9 March 2006*

*Amended: 8 May 2006*